System reliability of slopes using multimodal optimisation

Reale, C.; Xue, J.; Gavin, K.

DOI
10.1680/jgeot.15.P.142

Publication date
2016

Document Version
Final published version

Published in
Geotechnique: international journal of soil mechanics

Reale, C. *et al.* (2016). *Géotechnique* **66**, No. 5, 413–423 [http://dx.doi.org/10.1680/jgeot.15.P.142]

System reliability of slopes using multimodal optimisation

C. REALE*†, J. XUE‡ and K. GAVIN*†

Many engineered and natural slopes have complex geometries and are multi-layered. For these slopes traditional stability analyses will tend to predict critical failure surfaces in layers with the lowest mean strength. A move toward probabilistic analyses allows a designer to account for uncertainties with respect to input parameters that allow for a more complete understanding of risk. Railway slopes, which in some cases were built more than 150 years ago, form important assets on the European rail network. Many of these structures were built at slope angles significantly higher than those allowed in modern design codes. Depending on the local geotechnical conditions these slopes may be susceptible to deep-seated failure; however, a significant number of failures each year occur as shallow translational slips that develop during periods of high rainfall. Thus, for a given slope, two potential failure mechanisms might exist with very similar probabilities of failure. In this paper a novel multimodal optimisation algorithm ('Slips') that is capable of detecting all feasible probabilistic slip surfaces simultaneously is presented. The system reliability analysis is applied using polar co-ordinates, as this approach has been shown to be less sensitive to local numerical instabilities, which can develop due to discontinuities on the limit state surface. The approach is applied to two example slopes where the complexity in terms of stratification and slope geometry is varied. In addition the methodology is validated using a real-life case study involving failure of a complex slope.

KEYWORDS: embankments; landslides; limit equilibrium methods; numerical modelling; slopes; statistical analysis

INTRODUCTION

Within the geotechnical engineering community the significant uncertainties associated with slope stability analyses mean that the area has been at the forefront of the application of reliability-based design approaches, (see Whitman & Bailey, 1967; Christian *et al.*, 1994; Juang *et al.*, 1998; Malkawi *et al.*, 2000; Baecher & Christian, 2005). Although a range of uncertainties exist when designing new slopes or in the evaluation of existing slopes, the principal uncertainty which concerns geotechnical engineers when evaluating slope stability involves quantifying the strength (and shear resistance) of the different soil layers. Owing to the extreme variability in most natural and man-made slopes, this uncertainty cannot be eliminated, or even reduced considerably, without unreasonable cost (Chowdhury & Xu, 1995).

Earth slopes are commonly used as flood defences, dams and as embankments and cuttings along road and rail networks. As a result, slope instability exposes members of the public to significant risk. To address this risk it is necessary to quantify accurately the disturbing force (applied loads, gravity forces and so on) and the capacity (which depends on the shear resistance along a potential failure surface) of a slope and associated uncertainties in order to predict failure zones as accurately as possible. Quantifying the load is a relatively simple task for most slopes, as there is reasonably little variation in soil and rock unit weights; as a result, gravitational loads and live loads due to traffic and so on can be quantified relatively accurately. However, the slope's capacity (resistance) is typically much harder to predict as the soil's shear strength can vary considerably, both spatially and temporally, due to water table level changes and the development of wetting fronts during periods of intense rain (Gavin & Xue, 2009). Given that the shear strength of a soil varies with moisture content (Fredlund & Rahardjo, 1993; Vanapalli *et al.*, 1996; Ridley *et al.*, 2004) and the moisture content is controlled by the climate it is subjected to, the effect of climate on near-surface soils is inherently uncertain. To deal with these uncertainties in deterministic design it is usual to adopt conservative fixed parameter values (Nguyen & Chowdhury, 1985). Although this approach has been used extensively, in practice it has significant drawbacks. In uniform soils adoption of conservative design values for parameters can be excessively conservative, whereas for highly variable soils the fixed parameter values selected may not adequately encapsulate the level of variability present and unsafe designs can result (Morgenstern, 2000). An additional consideration is that the design of effective remediation strategies becomes increasingly challenging when real slope behaviour is not accurately modelled. As a result, over recent decades significant research has been carried out investigating the application of reliability methods to slope stability problems (Christian *et al.*, 1994; Low & Tang, 1997; Low *et al.*, 1998; Hassan & Wolff, 1999; Babu & Murthy, 2005; Gavin & Xue, 2009) where variables are described by distributions instead of fixed values. These approaches have the inherent benefit of allowing designers to quantify the level of uncertainty present and significantly reduce risk. A thorough review of uncertainty and variability in geotechnical engineering can be found in Phoon & Kulhawy (1999a, 1999b) and Baecher & Christian (2005), and a number of reviews have been carried out on reliability analysis as it pertains to geotechnical engineering (Phoon, 2008; Cheng *et al.*, 2015; Reale *et al.*, 2016).

In general, probabilistic methods can be classified into two separate categories: approximate methods such as first-order second moment (FOSM) and simulation-based approaches

Manuscript received 1 June 2015; revised manuscript accepted 19 November 2015. Published online ahead of print 18 January 2016.
Discussion on this paper closes on 1 October 2016, for further details see p. ii.
* School of Civil Engineering, University College Dublin, Ireland.
† Earth Institute, University College Dublin, Ireland.
‡ School of Applied Sciences and Engineering, Federation University Australia, Churchill, Victoria, Australia.

such as the Monte Carlo method. Over recent years with advances in computing power there has been renewed interest in simulation methods, with numerous authors proposing quasi Monte Carlo methods (Malkawi *et al.*, 2001; Wang *et al.*, 2011; Cheng *et al.*, 2015) as a means of finding the critical probabilistic slip surface. Simulation techniques can be used to find both the system reliability (Griffiths & Fenton, 2004; Huang *et al.*, 2010) and the reliability index for a given slip surface. However, this paper proposes an alternative approximate technique for rapidly finding the system reliability of a slope with multiple failure mechanisms.

To date, the majority of applications of probabilistic analysis to slope stability problems have involved a two-step decoupled approach. In the first step the location of the critical slip surface is established using a deterministic approach. In the second step a probabilistic analysis is performed wherein the critical inputs are described using some appropriate statistical distribution to obtain the critical reliability index. However, as the slip surface in question is still the deterministic critical slip surface, this approach is unlikely to find the true minimum reliability index. Over recent years researchers (Hassan & Wolff, 1999; Bhattacharya *et al.*, 2003; Xue & Gavin, 2007, among others) have incorporated sophisticated techniques to search simultaneously for the critical probabilistic surface and critical design points of input parameters, allowing for a more accurate minimum reliability index. These approaches represent a significant advance on earlier approaches, but they still only provide the user with the most critical slip surface (lowest reliability index) for a given slope condition or state. This is clearly unsatisfactory, as over the design life of a slope its condition (water table position, degree of saturation and so on) will change. For example, for a slope where deep-seated and shallow failures have similar likelihoods of occurrence, although a deep-seated failure mode might be more likely during the dry season, during a period of prolonged rainfall a shallow slip might develop and both failure modes should be identified in an analysis. Furthermore, large slopes with complex geometries (e.g. multiple benches) can have multiple viable failure surfaces with similar failure probabilities, the criticality of which is typically determined by the triggering mechanism which presents itself first.

To address this deficit, the current paper uses a novel optimisation method, 'Slips' (standardised locally informed particle swarm), which is able to simultaneously converge to multiple different optima through the use of a sophisticated niching algorithm. When combined with a suitable limit state and first-order reliability method ('Form') this allows for the location of multiple distinct 'critical' probabilistic slip surfaces and the simultaneous determination of their related reliability indices. A polar co-ordinate defined search space is used instead of the more traditional Cartesian co-ordinate system, as this has been shown to be less sensitive to local discontinuities on the limit state surface (Val *et al.*, 1996). As most slopes have multiple viable slip surfaces, the overall failure probability of the slope as a system should be evaluated, not just that of the critical failure surface; the probability of failure of the critical failure surface may be significantly less than that of the slope as a whole (Oka & Wu, 1990; Chowdhury & Xu, 1995; Huang *et al.*, 2010; Zhang *et al.*, 2011; Ji & Low, 2012). Therefore, this paper considers the correlation between different viable slip surfaces and uses that correlation to determine upper and lower bounds for the system's probability of failure. Non-circular slip circles are used as these allow a wider range of potential slip surface shapes to be adopted, ranging from translational slips, which typically present as a shallow wetting front depth (usually less than 2 m deep) and which form parallel to the slope surface, to the circular or near-circular surface associated with deep-seated failures. The model is applied to three case studies and the results are discussed in the final section.

METHODOLOGY

General overview of reliability-based design

Reliability methods provide a framework which allows designers to incorporate uncertainty into stability calculations and thereby offer a more meaningful interpretation of safety than deterministic calculations. The performance function ($g(\boldsymbol{X})$) or limit state function of a slope can be expressed as the difference between the capacity (C) and demand (D), see equation (1).

$$g(\boldsymbol{X}) = (C - D)\begin{cases} > 0, & \text{safe state} \\ = 0, & \text{limit state} \\ < 0, & \text{failure state} \end{cases} \qquad g(\boldsymbol{X}) = g(x_1,\ x_2,\ \ldots\ , x_n) \quad \text{for } i = 1 \text{ to } n \tag{1}$$

where $\boldsymbol{X}$ is the vector of the different random variables (x_i) in the problem. A reliability analysis typically provides two equivalent measures of safety: a reliability index, β, and a probability of failure, P_f. The probability of failure is defined as the probability of the performance function being less than zero, see equation (2).

$$P_f = P[g(\boldsymbol{X}) \leq 0] \tag{2}$$

The reliability index is defined as the distance in standard deviations from the mean of the performance function to the design point, equation (3).

$$\beta = \frac{E[g(\boldsymbol{X})]}{\sigma[g(\boldsymbol{X})]} \tag{3}$$

where $E[g(\boldsymbol{X})]$ is the mean of the performance function at the design point (critical slip surface) and $\sigma[g(\boldsymbol{X})]$ is its standard deviation, see Fig. 1. When performing slope stability analyses the performance function of the slope is typically presented in the form shown in equation (4).

$$g(\boldsymbol{X}) = \text{FOS} - 1{\cdot}0 \tag{4}$$

where FOS is the factor of safety.

First-order reliability methods (Form)

In a Form analysis all random variables ($\boldsymbol{X}$) that define the performance function $g(\boldsymbol{X})$ are first transformed into the

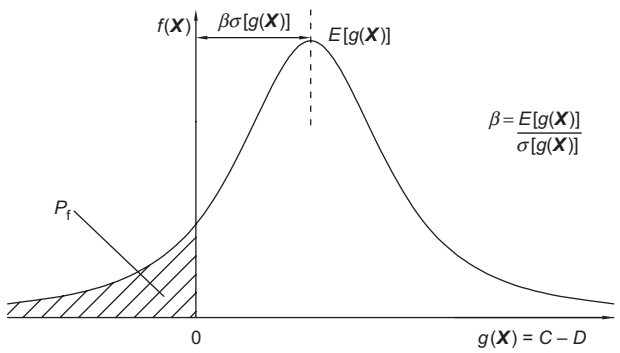

Fig. 1. Relationship between reliability index, probability of failure and performance function for a normally distributed performance function

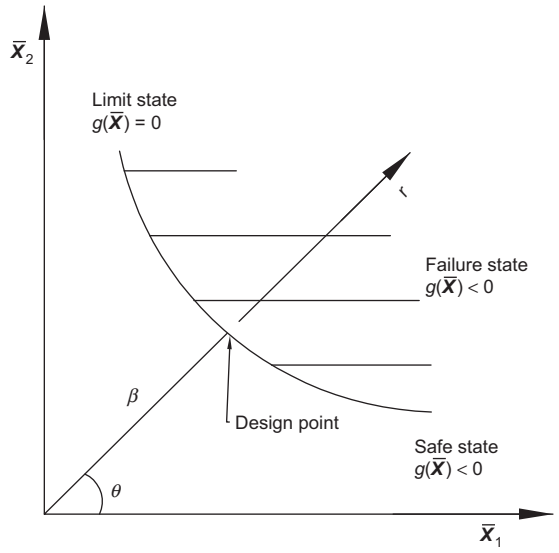

Fig. 2. Relationship between design point and reliability index for a 'Form' analysis

standard normal space ($\bar{\boldsymbol{X}}$), see Fig. 2. In this reduced variable space ($\bar{\boldsymbol{X}}$), the reliability index, β, is equivalent to the minimum distance from the origin to the limit state surface defined by $g(\bar{\boldsymbol{X}}) = 0$. Traditionally this distance was determined by performing a cosine directional search along the limit state surface. However, Val *et al*. (1996) noted that this technique was unlikely to locate the minimum reliability index when considering non-linear performance functions. Following the work of Val *et al*. (1996), Xue & Gavin (2007) described a method that transforms the standardised variables described in equation (4) from Cartesian co-ordinates into polar coordinates using radial distance (r) and polar angles ($\theta_1, \theta_2, \ldots, \theta_{N-1}$). In this paper the non-circular slip model is expanded to account for multimodal system reliability. The polar coordinates at the design point for a number of variables can be described using equations (5) and (6), where N is the number of variables -1. Fig. 2 shows the process diagrammatically.

$$\bar{X}_i = r\omega_i \tag{5}$$

where $\omega_i = \sin\ \theta_{N-i+1} \Pi_{i=1}^{N-i} \cos\ \theta_i$ and is equivalent to the directional cosine vector typically used in Form analyses; therefore

$$\bar{X}_i = r \sin\ \theta_{N-i+1} \Pi_{i=1}^{N-i} \cos\ \theta_i, \quad i = 1, 2, \ldots, N \tag{6}$$

where $\sin\ \theta_N = 1$, and

$$(-1/2)\pi \leq \theta_i \leq (1/2)\pi$$
$$(i = 1, 2, \ldots, N-2),\ 0 \leq \theta_{N-1} \leq 2\pi$$

The reliability index is then defined by equation (7) where $\bar{\boldsymbol{X}}$ is the vector of reduced variables described in equation (6).

$$\beta = \min_{\bar{\boldsymbol{X}} \epsilon \psi} \left(\bar{\boldsymbol{X}}^{\mathrm{T}} \bar{\boldsymbol{X}} \right)^{1/2} \tag{7}$$

System reliability in polar coordinates

A system may have multiple distinct failure modes or limit states; in such circumstances the exceedance of any individual limit state constitutes a system failure. In terms of slopes stability this means that there are many potential slip surfaces present within the slope. These failure surfaces may or may not be interdependent, that is, some slip surfaces may overlap while others may be considered as independent events. Therefore, to evaluate system reliability, the correlation between the different possible failure modes (ρ_{ij}) needs to be determined. Ji & Low (2012) suggest ρ_{ij} can be obtained from the following relationship between Cartesian design points and failure mode correlation coefficients.

$$\rho_{ij} = \frac{\bar{X}_i^{\mathrm{T}} \bar{X}_j}{\beta_i \beta_j} \tag{8}$$

Transforming equation (8) into polar form using equation (5) the correlation coefficient between failure modes i and j becomes

$$\rho_{ij} = \frac{(r\omega)_i^{\mathrm{T}} (r\omega)_j}{\beta_i \beta_j} \tag{9}$$

However, from Fig. 2 it can be seen that at the design point $r = \beta$, therefore at the design point equation (9) reduces to equation (10).

$$\rho_{ij} = \omega_i^{\mathrm{T}} \omega_j \tag{10}$$

Extrapolating equation (10) to account for all failure modes, the correlation matrix ($\boldsymbol{\rho}$) for the entire system can be evaluated using equation (11), where $\boldsymbol{\omega}$ is a vector containing all possible failure modes.

$$\boldsymbol{\rho} = \boldsymbol{\omega}^{\mathrm{T}} \boldsymbol{\omega} \tag{11}$$

Kounias (1968) and Ditlevsen (1979) suggested a bimodal bounded approach for estimating the system probability of failure ($P_{\mathrm{f,sys}}$) for systems with several failure modes. Ma & Ang (1981) note that these bounds are typically reasonably narrow except for situations where numerous individual failure modes have large failure probabilities (e.g. $p_{\mathrm{f}} > 10^{-2}$). The approach presented in equation (12) requires the probability of failure and correlation of all failure modes to have been evaluated prior to computation. The failure modes and corresponding correlation matrix should be sorted from most likely ($P_{\mathrm{f,max}}$) to least likely ($P_{\mathrm{f,min}}$) in order to provide the narrowest possible probability bounds (Ang & Tang, 1984; Haldar & Mahadevan, 2000).

$$\begin{aligned} P_{\mathrm{f,max}} + \max \sum_{i=2}^{m} \left[P_{\mathrm{f}}(i) - \sum_{j=1}^{i-1} P_{\mathrm{f}}(i,j);\ 0 \right] \\ \leq P_{\mathrm{f,sys}} \\ \leq \min \left[\sum_{i=1}^{m} P_{\mathrm{f}}(i) - \sum_{i=2}^{m} \max_{j<i} P_{\mathrm{f}}(i,j);\ 1 \right] \end{aligned} \tag{12}$$

where $P_{\mathrm{f}}(i,j)$ represents the probability of both failure modes i and j occurring simultaneously. Depending on the correlation between failure modes this term can be substantial but is notoriously difficult to evaluate. Ditlevsen (1979) proposed a simplified methodology for evaluating this term provided all inputs used were Gaussian random variables, see equations (13) and (14).

$$\max[a, b] \leq P_{\mathrm{f}}(i,j) \leq a + b, \quad \text{for } \rho_{i,j} > 0 \tag{13a}$$

$$0 \leq P_{\mathrm{f}}(i,j) \leq \min[a, b], \quad \text{for } \rho_{i,j} < 0 \tag{13b}$$

where a and b are defined as follows

$$a = \Phi(-\beta_i) \Phi\left(-\frac{\beta_j - \rho_{ij}\beta_i}{\sqrt{1 - \rho_{ij}^2}} \right) \tag{14a}$$

$$b = \Phi\left(-\beta_j\right)\Phi\left(-\frac{\beta_i - \rho_{ij}\beta_j}{\sqrt{1-\rho_{ij}^2}}\right) \tag{14b}$$

This reduces the complexity of the problem to a straightforward computation of the reliability indices of individual failure modes and their corresponding correlation coefficients, thus allowing the user to obtain an upper and lower bound estimate for $P_{\text{f,sys}}$. Low *et al.* (2011) provide a VBA (visual basic for applications) code for easy computation of equations (13) and (14).

Non-circular slip surfaces

The limit state equation adopted in this paper is Bishop's simplified method adapted for non-circular slip surfaces, see equation (15). However, it is important to note that a wide variety of slope stability limit equilibrium methodologies (LEMs) exist and, depending on the situation, a different LEM may be more applicable. For example, as Bishop's simplified method does not consider horizontal force equilibrium, it should not be applied to situations where horizontal forces might be significant (e.g. earthquake loading). Horizontal loads could be easily incorporated in the methodology presented through the use of a different failure model. An extensive review of LEMs suitable for slope stability analysis can be found in Fredlund & Krahn (1977). Bishop's non-circular model was used in this study as it can accommodate failure planes developing parallel to the slope's surface, along weak layers, as well as the more classical circular slip shape. When used in conjunction with a multimodal search algorithm this allows for better assessment of stability and makes it less likely that an important failure mode could be overlooked.

$$\text{FOS} = \frac{\sum_{i=1}^{n}[c_i\Delta x + (W_i - U_i)\tan(\phi_i)]\left\{\sec^2\alpha_i/[1+\tan(\phi_i)\tan\alpha_i]/\text{FOS}\right\}}{\sum_{i=1}^{n} W_i \tan\alpha_i} \tag{15}$$

where n is the number of slices; Δx is the slice width; α_i is the inclination angle of the base of the slice; W_i is the weight of the slice; U_i is the positive pore pressure within the slice if the water table is above the base of the slice; c_i is the cohesion value and ϕ_i is the internal angle of friction, both taken at the mid-point of the base of the slice.

The performance function is shown in equation (16). The FOS term in equation (15) reduces to 1 at the limit state.

$$G(\boldsymbol{X}) = \frac{\sum_{i=1}^{n}[c_i\Delta x + (W_i - U_i)\tan(\phi_i)]\left\{\sec^2\alpha_i/[1+\tan(\phi_i)\tan\alpha_i]\right\}}{\sum_{i=1}^{n} W_i \tan\alpha_i} - 1 \tag{16}$$

The following constraints are necessary in order for a successful optimisation to occur; they are described in greater detail in Xue & Gavin (2007)

$$\begin{cases} (-1/2)\pi \le \theta_i \le (1/2)\pi & (i = 1,2,\ldots,2k-2) \\ 0 \le \theta_{2k-1} \le 2\pi & \\ x_n - x_0 \ge 0 & \\ \dfrac{\sec\alpha_i}{1+\tan\phi_i\tan\alpha_i} \ge 0{\cdot}2 & (i = 0,1,2,\ldots,n-1) \\ \text{Px}(x_i) - y_i \ge 0 & (i = 1,2,\ldots,n-1) \\ y_i - H \ge 0 & (i = 1,2,\ldots,n-1) \\ E(c_i) + r\omega_i\sigma(c_i) \ge 0 & (i = 1,2,\ldots,k) \\ E[\tan(\phi_i)] + r\omega_{k+i}\sigma[\tan(\phi_i)] \ge 0 & (i = 1,2,\ldots,k) \end{cases}$$

where k represents the soil layer in question; H is the height to a hard stratum; y is the height of the slip; and Px is the function which describes the slope profile. Fig. 3 depicts these parameters graphically.

Optimisation procedure

The proposed optimisation procedure Slips (standardised locally informed particle swarm) is an enhanced version of an optimisation model previously used by the authors termed 'Lips' – locally informed particle swarm (Qu *et al.*, 2013; Reale *et al.*, 2015). These are both variations of particle swarm optimisation (PSO) which have been adapted to enhance their ability to solve multimodal problems. An overview of PSO algorithms is provided below. A more in-depth understanding of PSO algorithms can be gained by reading Kennedy (2010).

Particle swarm algorithms. Eberhart & Kennedy (1995) developed an optimisation method based on the social organisation of swarm animals (birds, fish and so on), which seek food collaboratively, termed PSO. In PSO, each particle in the swarm represents a solution to an optimisation problem. In deference to evolutionary algorithms, PSO particles do not use mutation, crossover or breeding to optimise (see Xue & Gavin, 2007); therefore, all particles survive until the end of the optimisation. This can be a drawback if particles are initially located far from a minimum, as there is no shortcut to the solution and particles will have to move there iteratively. The swarm contains a predetermined number of particles, each of which moves with a velocity about the search space seeking a better solution (in this case minimum β). In every iteration, each particle updates both its position (U) and velocity (V) based on both that particle's individual best experience (lowest β) so far (local extrema, termed 'pbest') and the swarm's best experience so far (global extrema, termed 'gbest'). When a particle is in the locale of a local or global minimum it slows down; if there is no minimum present, the particle increases its velocity and moves to a different area of the search space. Whenever a particle iterates to a better pbest than the current gbest, that particle turns into the new gbest. The old gbest is then demoted to the status of a local minimum. In this way every particle is constantly aware of the most 'profitable' areas of the search space.

The position U and velocity V of each particle are calculated using the following equations (17) and (18)

$$V_{i,d}^{t+1} = \vartheta\, V_{i,d}^{t} + c_1\,\text{rand1}_{i,d}\left(\text{pbest}_{i,d} - U_{i,d}^{t}\right) + c_2\,\text{rand2}_{i,d}\left(\text{gbest}_{i,d} - U_{i,d}^{t}\right) \tag{17}$$

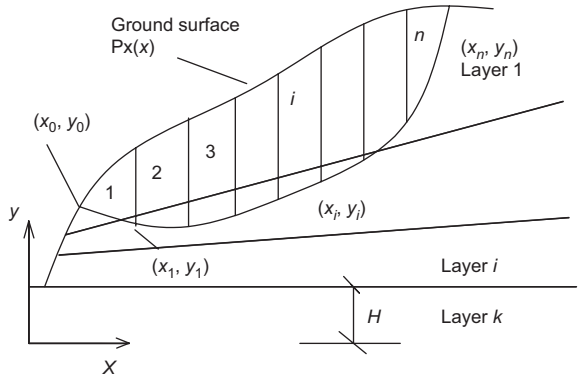

Fig. 3. Various parameters used to define non-circular slip circles in a slope with *k* layers (Xue & Gavin, 2007)

$$U_{i,d}^{t+1} = U_{i,d}^{t} + V_{i,d}^{t} \tag{18}$$

where i is the target particle's index, d is the dimension of the search space, c_1 and c_2 are constants controlling the particle's acceleration; $\text{pbest}_{i,d}$ represents a particle i's best position to date; $\text{gbest}_{i,d}$ represents the swarm's best position to date; ϑ is the inertia weight which balances the search between global and local performance. The value assigned to ϑ is important, as it prevents particles from quickly abandoning search in their respective area every time the gbest is updated; $\text{rand1}_{i,d}$ and $\text{rand2}_{i,d}$ are random numbers between 0 and 1.

A deficiency of PSO when applied to multimodal problems is that every particle is updated with the position of the global optimum solution, therefore given sufficient generations every particle ends up being drawn to the global minimum.

Standardised locally informed particle swarm optimisation (Slips)

In multimodal problems, numerous global or near-global optima exist; however, most optimisation models are only capable of searching for one extrema per run. Traditionally multimodal problems required optimisation techniques to be run several times to find all solutions. This requires substantial user intervention to ensure previous solutions are screened out of the search space to prevent reoccurrence. Therefore, solving multimodal problems can be a laborious task using traditional techniques. By defining several sub-swarms, numerous PSO-based algorithms (Qu & Suganthan, 2010; Qu *et al*., 2012) have been able to define stable niches within the search space, which facilitates optimising to multiple peaks. Qu *et al*. (2013) developed a variant of PSO, termed 'Lips', which differs from standard PSO in that each particle within the swarm is only allowed to share information with other particles in its neighbourhood. In this instance, a neighbourhood is defined as the nsize closest particles to the particle in question, measured in Euclidian distance. This limits the number of particles which are aware of the location of the global best. Instead each particle is aware of its personal best solution (pbest) and that of its neighbourhood, thus easily facilitating the development of distinct niches within the search space. This means that every particle can learn from those around it, but its search cannot be altered by particles on the opposite side of the search space.

Reale *et al*. (2015) successfully adapted this optimisation procedure to solve probabilistic slope stability problems using Bishop's circular slip surface. However, when the optimisation procedure was applied to non-circular slip surfaces the optimisation process became erratic, as there were substantially more variables to be optimised. The algorithm's poor performance when presented with higher-dimensional data can be attributed to the difficulty in determining each particle's nearest neighbours. This is partly owing to the scale effect of increased dimensions, but is primarily a result of the optimisation variables being of different type (material and geometric) and hence scale; that is, the variables measured in large-valued units dominate the search process. This problem was overcome by modifying the Lips algorithm to determine the nearest neighbours using standardised or normalised Euclidian distance instead of Euclidian distance. By using standardised Euclidian distance to measure nearest neighbours, the difference in scale between the different dimensions is no longer an influencing factor, as the standard space is scale invariant and unitless. This updated algorithm is termed Slips. The standardised Euclidean distance between two particles A and B can be calculated using equation (19), where s_i is the sample standard deviation of the neighbourhood containing particles a and b.

$$\text{dist}(A, B) = \sqrt{\sum_{i=1}^{N} \frac{(A_i - B_i)^2}{s_i^2}} \tag{19}$$

The equations to update the velocities (V) and positions (U) of the particles remain the same as those used in the Lips algorithm, equations (18)–(21). Table 1 describes the optimisation process.

$$V_{i,d}^{t+1} = \vartheta \left[V_{i,d}^{t} + \varphi \left(P_{i,d}^{t} - U_{i,d}^{t} \right) \right] \tag{20}$$

$$P_{i,d}^{t} = \frac{\sum_{j=1}^{\text{nsize}} \left(\varphi_j \, \text{nbest}_j \right) / \text{nsize}}{\varphi} \tag{21}$$

where φ_j is a random distributed number in the range of $[0, (4{\cdot}1)/\text{nsize}]$ and φ is equal to the summation of φ_j; nbest_j is the jth nearest neighbourhood to the ith particle's personal best (pbest); nsize is the neighbourhood size; and ϑ is the inertia weight which balances the search between global and local performance. The optimisation process is terminated when the function evaluations limit is reached. The function evaluations limit is the maximum number of times the velocity and position vectors are updated for each particle. Its value should be sufficiently high to obtain a repeatable level of accuracy, to the desired number of decimal places. The greater the number of optima to be located within the search space, the larger the function evaluations limit should be. If the search space is complex, the particle population and function evaluations limit should be increased to improve accuracy.

Table 1. Slips schema

Step 1	Randomly generate initial solutions
Step 2	Evaluate the initial pbests for the entire population (n) For $i = 1{:}n$
Step 3	Establish neighbourhood of nsize particles for ith particle using equation (19)
Step 4	Identify the neighbourhood best for ith particle.
Step 5	Update the particles velocity (equation (18))
Step 6	Update the particles position (equation (17))
Step 7	Evaluate new ith particle solution
Step 8	Update ith particle pbest End for
Step 9	Terminate if stopping criteria are met otherwise repeat from step 3

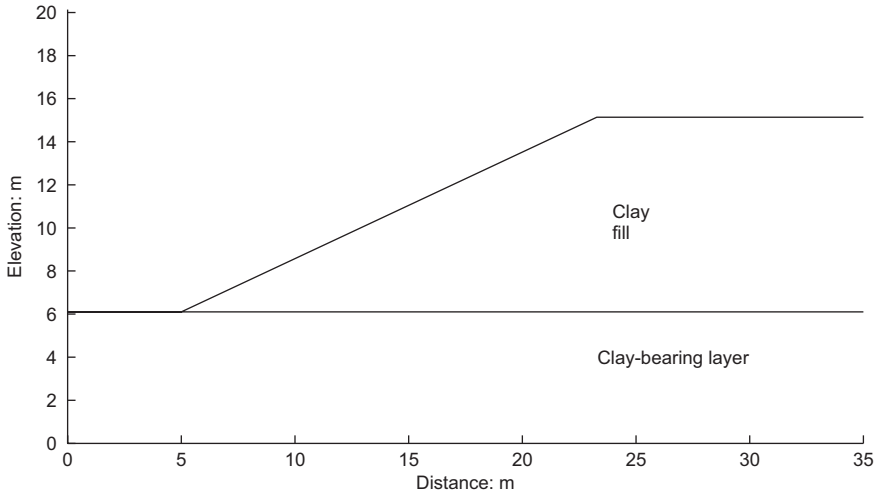

Fig. 4. Geometry chosen for case study 1

RESULTS AND DISCUSSION

Case study 1: railway embankment

A 10 m high embankment composed of soft clay fill founded on a stiffer clay deposit was chosen for this case study. The embankment is inclined at 26·5° to the horizontal, see Fig. 4. The soil properties used for the case study are summarised in Table 2. Normal distributions were used to model all parameters. The Slips model detected four representative slip surfaces, shown in Fig. 5; of these four slip surfaces, three passed through the fill layer into the underlying stiff clay-bearing layer. These slip surfaces all had reliability indices greater than 2·4 and could be considered reasonably safe. However, the critical slip surface stayed within the weaker embankment fill and as a result had a significantly lower reliability index of 1·0. This corresponds to a failure probability of 0·1587. The correlation coefficients between the slip surfaces (e.g. between m_1 and m_2, and so on) were calculated using equation (11) and the results are shown in Table 3, together with the bounds for system probability of failure. Owing to the large discrepancy in safety between the different failure modes the system probability of failure bounds (see Table 3) are reasonably narrow and are heavily influenced by the critical failure mode. The co-ordinates of the detected slip circles and polar angle design points are given in Table 4.

Case study 2: multi-layered embankment

The second case study outlined here is a hypothetical example of a large, multi-layered embankment with a berm. The embankment consists of two well-defined fill layers overlying a 10 m deep deposit of stiff glacial till. The geometry used in this example is shown in Fig. 6 and the soil properties are summarised in Table 5. Normal distributions were used to model all parameters. The water table was assumed to be at the top of the glacial till layer.

Slips detected five distinct failure modes, which can be seen in Fig. 7. The most likely failure mode was found to be a relatively small slide, which did not affect fill layer 1. It had a minimum reliability index of 3·41, which was substantially less than the four other failure modes detected, see Table 6. Therefore, similarly to case study 1, the failure probability of the critical slip surface ($3{\cdot}2146 \times 10^{-4}$) has a massive influence on the system probability bounds. As a result there is virtually no difference in this example between the

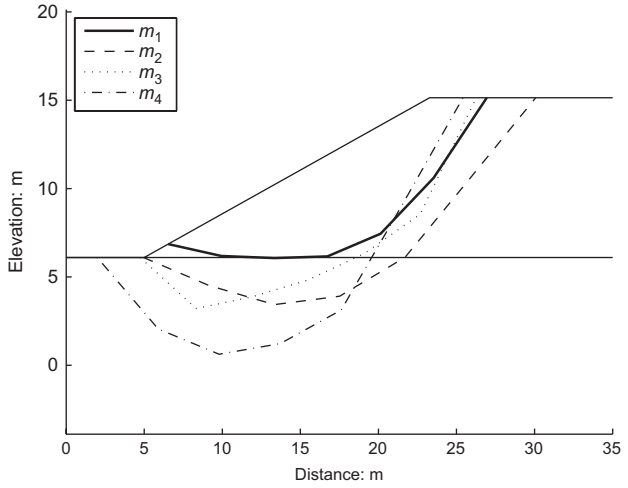

Fig. 5. Representative non-circular failure modes detected using Slips

Table 2. Soil properties and associated uncertainties for case study 1

	Clay fill			Clay-bearing layer		
	c': kPa	ϕ: deg	γ: kN/m^3	c': kPa	ϕ: deg	γ: kN/m^3
Mean	10	10	18	25	12	18
Std deviation	2	1	—	5	1·2	—
Coefficient of variation	0·2	0·1	—	0·2	0·1	—

Table 3. Failure mode correlation matrix, reliability indices and system probability of failure bounds for case study 1

Failure mode	Correlation matrix, **ρ**				β
	m_1	m_2	m_3	m_4	
m_1	1	0·6662	0·3199	0·5426	1·00
m_2	0·6662	1	0·7535	0·9293	2·40
m_3	0·3199	0·7535	1	0·8106	2·83
m_4	0·5426	0·9293	0·8106	1	3·33
System probability of failure bounds					
Lower: 0·1587			Upper: 0·1611		

Table 4. Co-ordinates of non-circular slip circles and polar thetas obtained from Slips for case study 1

Entry point: m	y_1: m	y_2: m	y_3: m	y_4: m	y_5: m	Exit point: m	θ_1	θ_2	θ_3	θ_4	β	Failure mode
6·54	6·19	6·07	6·16	7·44	10·61	26·94	1·21	0·28	0·65	0·95	1·00	1
4·96	4·52	3·43	3·91	6·10	10·61	30·07	0·50	0·86	0·52	1·01	2·40	2
4·74	3·21	3·88	4·83	6·32	8·55	26·27	0·14	0·84	0·49	0·46	2·83	3
1·99	2·06	0·62	1·22	3·12	9·06	25·42	0·39	1·15	0·44	1·32	3·33	4

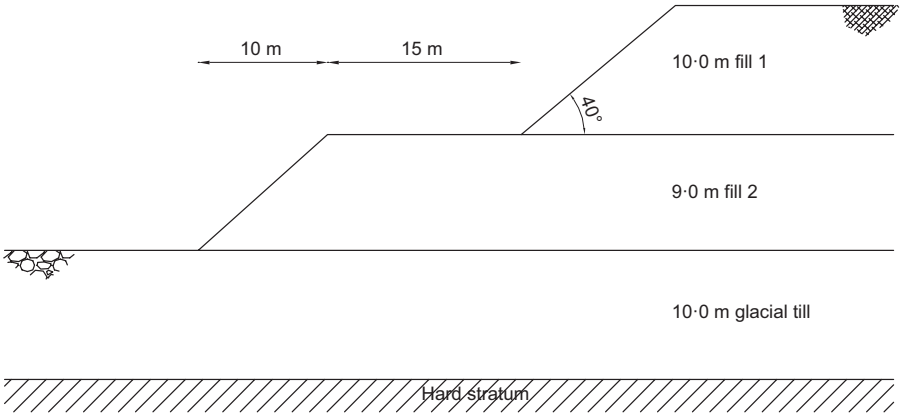

Fig. 6. Slope geometry for case study 2

Table 5. Soil properties and associated uncertainties for case study 2

	Fill 1			Fill 2			Glacial till		
	c': kPa	ϕ: deg	γ: kN/m^3	c': kPa	ϕ: deg	γ: kN/m^3	c': kPa	ϕ: deg	γ: kN/m^3
Mean	10	28	18	8	29	18·5	5	36	20
Std deviation	1	1·4	—	1·2	2·9	—	1	3·6	—
Coefficient of variation	0·1	0·05	—	0·15	0·1	—	0·2	0·1	—

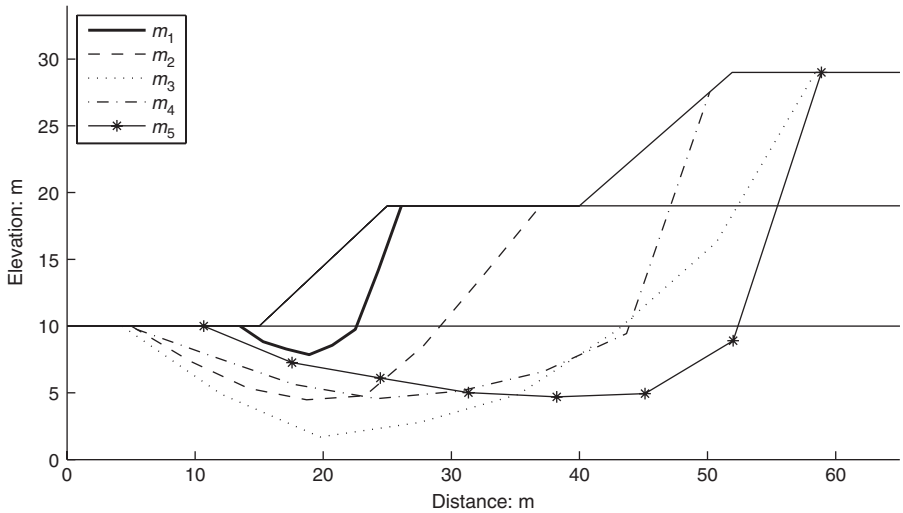

Fig. 7. Five most likely failure modes detected by the Slips algorithm

upper and lower system probability of failure bounds. The polar design points, slip circle y co-ordinates and entry and exit points for case study 2 can be found in Table 7.

Case study 3: Congress St Cut, Chicago

The Congress St Cut, Chicago cutting failure originally reported by Ireland (1954), has been extensively used as a validation case study in the literature (Oka & Wu, 1990; Chowdhury & Xu, 1995; Liang *et al.*, 1999, among others). The approximate profile of the cut is presented in Fig. 8. In this paper the shear strength of the three clay layers was modelled used normal distributions, and the strength of the sand fill layer was modelled using deterministic values, as it has negligible influence on the analyses. The material properties and associated uncertainties used in this example

Table 6. Correlation matrix showing the correlation indices between different slip modes and associated reliability indices. The resultant system failure probabilities are below

Failure modes	Correlation matrix, **ρ**					
	m_1	m_2	m_3	m_4	m_5	β
m_1	1	0·9625	0·9415	0·9411	0·9808	3·413
m_2	0·9625	1	0·9952	0·9929	0·9875	4·503
m_3	0·9415	0·9952	1	0·9982	0·9760	4·551
m_4	0·9411	0·9929	0·9982	1	0·9707	4·663
m_5	0·9808	0·9875	0·9760	0·9707	1	4·691
System probability of failure bounds: Lower: 0·00032146			Upper: 0·00032148			

Table 7. Co-ordinates of non-circular slip circles and polar thetas obtained from Slips for multi-layered embankment in case study 2

Entry point: m	y_1: m	y_2: m	y_3: m	y_4: m	y_5: m	y_6: m	Exit point: m	θ_1	θ_2	θ_3	θ_4	θ_5	θ_6	β	Failure mode
13·52	8·83	8·28	7·86	8·56	9·75	14·19	26·10	1·16	0·44	0·99	1·36	1·29	1·49	3·41	1
5·02	7·38	5·35	4·48	4·79	8·54	13·68	36·96	1·36	1·02	1·39	0·48	1·06	0·71	4·50	2
4·30	4·91	1·69	2·78	4·88	9·69	16·29	58·42	1·43	1·36	0·69	0·81	0·14	0·38	4·55	3
4·71	7·79	5·63	4·57	5·14	6·60	9·44	50·17	1·48	1·18	1·22	1·36	0·57	1·42	4·66	4
10·67	7·27	6·11	5·02	4·70	4·95	8·91	58·89	1·25	0·81	0·85	0·79	0·32	1·03	4·69	5

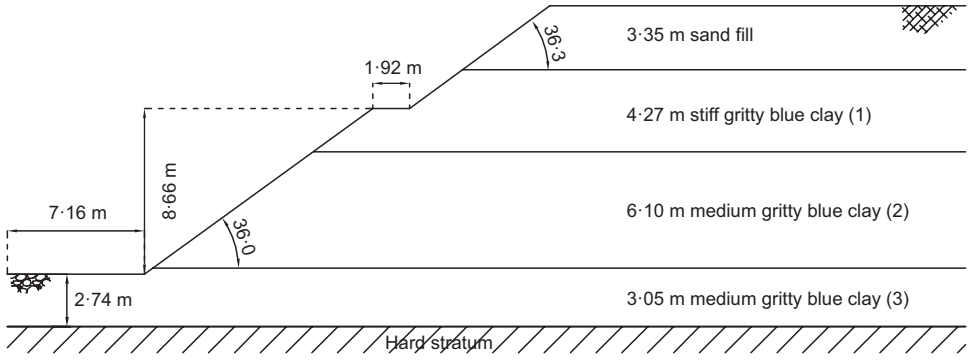

Fig. 8. Approximate profile of the Congress St Cut used in this example, dimensions taken from Ji & Low (2012)

Table 8. Soil properties and associated uncertainties for the Congress St Cut

	Sand fill		Clay 1	Clay 2	Clay 3
	c': kPa	ϕ: deg	c_u: kPa	c_u: kPa	c_u: kPa
Mean	—	30	55	43	56
Std deviation	—	—	20·4	8·2	13·2
Coefficient of variation	—	—	0·37	0·19	0·24

are presented in Table 8. The water table is assumed to be coincident with the base of the sand layer.

As a result of the analysis, five distinct slip surfaces were identified, see Fig. 9. The critical slip surface, m_1, was found to have a failure probability of 0·2921. The correlation matrix between the different slip surfaces and their reliability indices can be seen in Table 9. The slip circle co-ordinates' polar thetas following optimisation can be seen in Table 10. Owing to the presence of several slip surfaces with extremely poor reliability indices, the upper and lower system failure bounds are substantially different from one another. Furthermore, as

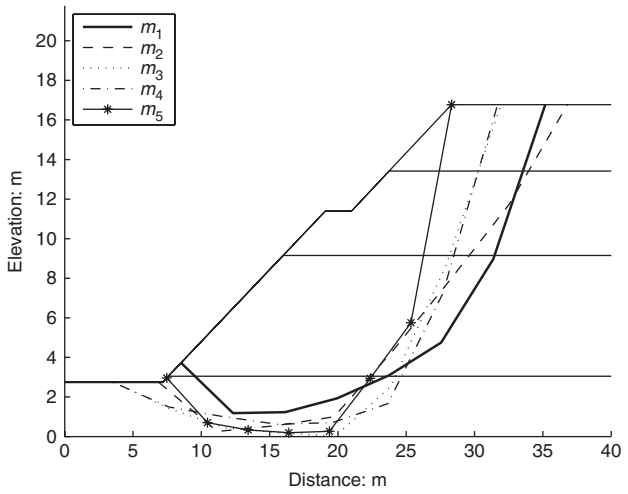

Fig. 9. Most probable failure modes determined by Slips algorithm

several near-critical slip surfaces exist, the lower bound failure probability of 0·32844 is considerably higher than that of the critical failure surface. The system upper bound of

Table 9. Failure mode correlation matrix, associated reliability indices and system probability of failure bounds

Failure modes	Correlation matrix, **ρ**					β
	m_1	m_2	m_3	m_4	m_5	
m_1	1	0·7278	0·4815	0·8088	0·6251	0·547
m_2	0·7278	1	0·8608	0·9750	0·9406	0·646
m_3	0·4815	0·8608	1	0·7672	0·8813	1·072
m_4	0·8088	0·9750	0·7672	1	0·8783	1·226
m_5	0·6251	0·9406	0·8813	0·8783	1	1·756
System probability of failure bounds: Lower: 0·3284			Upper: 0·4757			

Table 10. Co-ordinates of non-circular slip circles and polar thetas obtained from Slips for Congress St Cut example

Entry point: m	y_1: m	y_2: m	y_3: m	y_4: m	y_5: m	y_6: m	Exit point: m	θ_1	θ_2	θ_3	β	Failure mode
8·52	1·19	1·23	1·93	3·10	4·75	8·97	35·18	0·48	0·73	1·24	0·55	1
6·89	0·26	0·55	1·00	4·31	7·95	11·73	36·80	1·14	1·26	1·13	0·65	2
3·61	1·41	0·44	0·19	0·02	2·51	8·62	31·94	1·19	0·08	0·15	1·07	3
3·56	1·50	1·01	0·62	0·71	1·66	7·22	31·69	0·92	1·31	1·41	1·23	4
7·47	0·71	0·33	0·19	0·27	2·94	5·75	28·32	1·21	0·58	0·44	1·76	5

0·47569 encapsulates the high level of variability in the system and emphasises the difference between analysing the probability of failure of a critical slip and that of the entire slope system for a slope with multiple critical slip surfaces.

The results compare well with the failure bounds obtained by Chowdhury & Xu (1995) of [0·27389, 0·44733]. They employed a similar approach to calculate the bimodal system bounds, but obtained their critical slip surfaces by performing multiple deterministic analyses using the conjugate gradient method. Ji & Low (2012) obtained a system probability of failure of 0·3911 by performing Monte Carlo simulations on their stratified response surfaces using sample sizes of 50 000. One reason for the slightly higher probabilities of failure predicted by Slips might be the use of Bishop's non-circular limit state, which is known to give slightly lower factors of safety than Bishop's circular slip surface.

CONCLUSION

This paper presents a novel multimodal optimisation model termed 'Slips', which is able to simultaneously locate multiple distinct non-circular probabilistic failure surfaces within a slope. It accomplishes this by establishing multiple sub-swarms through a sophisticated niching algorithm, which allows it to converge to multiple different optima. Although some existing optimisation methods have accomplished similar solutions for deterministic analyses and for probabilistic circular slip surfaces, the authors are not aware of any existing non-circular multimodal reliability analyses. Multimodal non-circular probabilistic slip surfaces involve significantly more optimisation variables than circular probabilistic slip surfaces and as a result require additional computational power. However, non-circular slip surfaces offer several advantages over circular slip surfaces in that they can emulate multiple different failure shapes, such as parallel failures, circular failures and failures along weak layers. This is a significant advantage when trying to locate all possible failure modes within a slope.

Many slopes have multiple viable failure surfaces with similar failure probabilities. Therefore, when analysing existing marginal slopes it is imperative to consider the presence of multiple critical or near-critical failure planes; missing any could make potential rehabilitation measures redundant. Furthermore, for slopes which are susceptible to climate effects, the critical failure mode may vary over relatively short time periods; for example, during heavy rainfall a reduction in near-surface suctions could cause the development of a preferential shallow slip surface. Therefore, when modelling slope stability, designers should consider the stability of the slope as a whole system instead of examining solely the stability of the most critical slip surface.

This paper also demonstrates how to perform a system reliability analysis using polar co-ordinate defined reduced random variables. A formula is provided for generating the correlation matrix between the different failure modes in a polar co-ordinate search space. Once this correlation matrix has been obtained it can then easily be accommodated into Ditlevsen's bimodal bounded approach for estimating system probability of failure.

Three case studies are examined using this methodology. In the first two case studies multiple distinct failure modes were found. However, in both examples there was one dominant failure mode which had a reliability index significantly less than the remaining failure modes. In such circumstances the system failure probability is unlikely to change much from that of the critical failure probability. This was shown to be the case in both case study 1 and 2.

In the third case study the Congress St Cut in Chicago was examined. The Slips algorithm detected a number of viable slip surfaces, including a slip surface (m_2, see Fig. 9) very similar to the actual slip surface recorded by Ireland. Owing to the significant number of viable slip surfaces, the probability of the system failing was shown to be substantially higher than that of the critical slip surface failing. The system failure probability bounds obtained compared favourably with those from the literature.

Although the analyses in this paper were carried out using Bishop's non-circular limit state and a polar co-ordinate defined search space, the Slips algorithm could easily be adapted to a Cartesian co-ordinate system and to accommodate other multimodal problems. It is important to note that the effects of spatial correlation structures on stability, such as those proposed by Le (2014) and Jamshidi Chenari & Alaie (2015), were neglected in this study and may be significant. Future work will address this.

ACKNOWLEDGEMENTS

The authors would like to acknowledge the support of the Earth and Natural Sciences (ENS) Doctoral Studies Programme, funded by the Higher Education Authority (HEA) through the Programme for Research at Third Level Institutions, Cycle 5 (PRTLI-5), co-funded by the European Regional Development Fund (ERDF) and the European Union Framework 7 Project Smart Rail (project no. 285683) and the Horizon 2020 Project Destination Rail (project no. 636285).

NOTATION

a, b	particles within a neighbourhood
c_i	cohesion value
c_1, c_2	constants
d	dimension of search space
E	mean
$g(\boldsymbol{X})$	performance function
H	height to hard stratum
i	target particle's index
N	number of variables − 1
n	number of slices
nsize	neighbourhood size
P_f	probability of failure
$P_{\mathrm{f,sys}}$	system probability of failure
Px	slope profile
r	radial distance to design point
U	particle position
U_i	positive pore pressure
V	particle velocity
W_i	weight of slice
$\bar{\boldsymbol{X}} = r\omega$	vector of reduced polar design points
x_n	exit point of slip circle
x_0	entry point of slip circle
y	height of slip
α_i	inclination angle of base of slice
β	reliability index
γ	soil unit weight
Δx	slice width
$\theta_1, \theta_2, \ldots, \theta_{N-1}$	polar angles describing location of design point
ϑ	inertia weight between global and local search
$\boldsymbol{\rho}$	correlation matrix between slip surfaces
σ	standard deviation
Φ	cumulative distribution function
ϕ_i	internal angle of friction
φ	summation of φ_j
φ_j	random distributed number in range of [0, (4·1)/nsize]
ω_i	$= \sin\theta_{N-i+1}\Pi_{i=1}^{N-i}\cos\theta_i$

REFERENCES

Ang, A. & Tang, W. (1984). *Probability concepts in engineering planning and design*. New York, NY, USA: Wiley.

Babu, G. S. & Murthy, D. (2005). Reliability analysis of unsaturated soil slopes. *J. Geotech. Geoenviron. Engng* **131**, No. 11, 1423–1428.

Baecher, G. B. & Christian, J. T. (2005). *Reliability and statistics in geotechnical engineering*. Chichester, UK: John Wiley & Sons.

Bhattacharya, G., Jana, D., Ojha, S. & Chakraborty, S. (2003). Direct search for minimum reliability index of earth slopes. *Comput. Geotech.* **30**, No. 6, 455–462.

Cheng, Y. M., Li, L. & Liu, L. L. (2015). Simplified approach for locating the critical probabilistic slip surface in limit equilibrium analysis. *Nat. Hazards Earth Syst. Sci. Discussions* **3**, No. 2, 1061–1112.

Chowdhury, R. & Xu, D. (1995). Geotechnical system reliability of slopes. *Reliability Engng Syst. Saf.* **47**, No. 3, 141–151.

Christian, J. T., Ladd, C. C. & Baecher, G. B. (1994). Reliability applied to slope stability analysis. *J. Geotech. Engng* **120**, No. 12, 2180–2207.

Ditlevsen, O. (1979). Narrow reliability bounds for structural systems. *J. Struct. Mech.* **7**, No. 4, 453–472.

Eberhart, R. & Kennedy, J. (1995). A new optimizer using particle swarm theory. In *MHS'95 – proceedings of the sixth international symposium on micro machine and human science*, Nagoya, Japan, pp. 39–43. Piscataway, NJ, USA: Institute of Electrical and Electronics Engineers.

Fredlund, D. G. & Krahn, J. (1977). Comparison of slope stability methods of analysis. *Can. Geotech. J.* **14**, No. 3, 429–439.

Fredlund, D. & Rahardjo, H. (1993). *Soil mechanics for unsaturated soils*. New York, NY, USA: John Wiley & Sons.

Gavin, K. & Xue, J. (2009). Use of a genetic algorithm to perform reliability analysis of unsaturated soil slopes. *Géotechnique* **59**, No. 6, 545–549, http://dx.doi.org/10.1680/geot.8.T.004.

Griffiths, D. V. & Fenton, G.A. (2004). Probabilistic slope stability analysis by finite elements. *J. Geotech. Geoenviron. Engng* **130**, No. 5, 507–518.

Haldar, A. & Mahadevan, S. (2000). *Probability, reliability, and statistical methods in engineering design*. New York, NY, USA: John Wiley & Sons.

Hassan, A. & Wolff, T. (1999). Search algorithm for minimum reliability index of earth slopes. *J. Geotech. Geoenviron. Engng* **125**, No. 4, 301–308.

Huang, J., Griffiths, D. & Fenton, G. (2010). System reliability of slopes by RFEM. *Soils Found.* **50**, No. 3, 343–353.

Ireland, H. O. (1954). Stability analysis of the congress street open cut in Chicago. *Géotechnique* **4**, No. 4, 163–168, http://dx.doi.org/10.1680/geot.1954.4.4.163.

Jamshidi Chenari, R. & Alaie, R. (2015). Effects of anisotropy in correlation structure on the stability of an undrained clay slope. *Georisk: Assessment Management Risk Engineered Syst. Geohazards* **9**, No. 2, 109–123.

Ji, J. & Low, B. K. (2012). Stratified response surfaces for system probabilistic evaluation of slopes. *J. Geotech. Geoenviron. Engng* **138**, No. 11, 1398–1406.

Juang, C. H., Jhi, Y. Y. & Lee, D. H. (1998). Stability analysis of existing slopes considering uncertainty. *Engng Geol.* **49**, No. 2, 111–122.

Kennedy, J. (2010). Particle swarm optimization. In *Encyclopedia of machine learning* (eds C. Sammut and G. I. Webb), pp. 760–766. New York, NY, USA: Springer.

Kounias, E. (1968). Bounds for the probability of a union, with applications. *Ann. Math. Statists* **39**, No. 6, 2154–2158.

Le, T. M. H. (2014). Reliability of heterogeneous slopes with cross-correlated shear strength parameters. *Georisk: Assessment Management Risk Engineered Syst. Geohazards* **8**, No. 4, 250–257.

Liang, R., Nusier, O. & Malkawi, A. (1999). A reliability based approach for evaluating the slope stability of embankment dams. *Engng Geol.* **54**, No. 3–4, 271–285.

Low, B. K. & Tang, W. H. (1997). Reliability analysis of reinforced embankments on soft ground. *Can. Geotech. J.* **34**, No. 5, 672–685.

Low, B., Gilbert, R. & Wright, S. (1998). Slope reliability analysis using generalized method of slices. *J. Geotech. Geoenviron. Engng* **124**, No. 4, 350–362.

Low, B., Zhang, J. & Tang, W. H. (2011). Efficient system reliability analysis illustrated for a retaining wall and a soil slope. *Comput. Geotech.* **38**, No. 2, 196–204.

Ma, H. & Ang, A. (1981). *Reliability analysis of redundant ductile structural systems*, report no. UILU-ENG-R1-201.3. Urbana-Champaign, IL, USA: University of Illinois Engineering Experiment Station.

Malkawi, A. I. H., Hassan, W. F. & Abdulla, F. A. (2000). Uncertainty and reliability analysis applied to slope stability. *Struct. Saf.* **22**, No. 2, 161–187.

Malkawi, A., Hassan, W. & Sarma, S. (2001). Global search method for locating general slip surface using Monte Carlo techniques. *J. Geotech. Geoenviron. Engng* **127**, No. 8, 688–698.

Morgenstern, N. (2000). *Performance in geotechnical practice*, The inaugural Lumb lecture. Hong Kong, China: Hong Kong University.

Nguyen, V. & Chowdhury, R. (1985). Simulation for risk analysis with correlated variables. *Géotechnique* **35**, No. 1, 47–58, http://dx.doi.org/10.1680/geot.1985.35.1.47.

Oka, Y. & Wu, T. (1990). System reliability of slope stability. *J. Geotech. Engng* **116**, No. 8, 1185–1189.

Phoon, K. (ed.) (2008). *Reliability-based design in geotechnical engineering: computations and applications*. Oxford, UK: Taylor and Francis.

Phoon, K. & Kulhawy, F. (1999a). Characterization of geotechnical variability. *Can. Geotech. J.* **36**, No. 4, 612–624.

Phoon, K. & Kulhawy, F. (1999b). Evaluation of geotechnical property variability. *Can. Geotech. J.* **36**, No. 4, 625–639.

Qu, B. & Suganthan, P. (2010). Modified species-based differential evolution with self-adaptive radius for multi-modal optimization. *Proceedings of the 2010 international conference on computational problem-solving (ICCP 2010)*, Li Jiang, China, pp. 326–331. Piscataway, NJ, USA: Institute of Electrical and Electronics Engineers (DVD).

Qu, B., Liang, J. & Suganthan, P. (2012). Niching particle swarm optimization with local search for multi-modal optimization. *Inf. Sci.* **197**, 131–143.

Qu, B., Suganthan, P. & Das, S. (2013). A distance-based locally informed particle swarm model for multimodal optimization. *Evolutionary Comput., IEEE Trans.* **17**, No. 3, 387–402.

Reale, C., Xue, J., Pan, Z. & Gavin, K. (2015). Deterministic and probabilistic multi-modal analysis of slope stability. *Comput. Geotech.* **66**, No. 5, 172–179.

Reale, C., Xue, J. & Gavin, K. (2016). Using reliability theory to assess the stability and prolong the design life of existing engineered slopes. In *Risk assessment and management in geotechnical engineering: from theory to practice*, geotechnical special publication in memory of the late Professor Wilson H. Tang. Reston, VA, USA: American Society of Civil Engineers, in press.

Ridley, A., McGinnity, B. & Vaughan, P. (2004). Role of pore water pressures in embankment stability. *Proc. Instn Civ. Engrs – Geotech. Engng* **157**, No. 4, 193–198.

Val, D., Bljuger, F. & Yankelevsky, D. (1996). Optimization problem solution in reliability analysis of reinforced concrete structures. *Comput. Structs* **60**, No. 3, 351–355.

Vanapalli, S., Fredlund, D. & Pufahl, D. (1996). The relationship between the soil-water characteristic curve and the unsaturated shear strength of a compacted glacial till. *Geotech. Testing J.* **19**, No. 3, 259–268.

Wang, Y., Cao, Z. & Au, S. K. (2011). Practical reliability analysis of slope stability by advanced Monte Carlo simulations in a spreadsheet. *Can. Geotech. J.* **48**, No. 1, 162–172.

Whitman, R. & Bailey, W. (1967). Use of computers for slope stability analysis. *J. Soil Mech. Found. Div.* **93**, No. 4, 475–498.

Xue, J. & Gavin, K. (2007). Simultaneous determination of critical slip surface and reliability index for slopes. *J. Geotech. Geoenviron. Engng* **133**, No. 7, 878–886.

Zhang, J., Zhang, L. & Tang, W. H. (2011). New methods for system reliability analysis of soil slopes. *Can. Geotech. J.* **48**, No. 7, 1138–1148.